Report No. 00/3

CHALMERS UNIVERSITY OF TECHNOLOGY

Department of Thermo and Fluid Dynamics

Large-eddy simulations of turbulent flows in stationary and rotating channels and in a stationary square duct

by

Jordi Pallares and Lars Davidson

Gothenburg, 2000

ABSTRACT

Turbulent flows at low Reynolds numbers in stationary and rotating channels were simulated using the large-eddy simulation technique and compared with direct numerical simulations (DNS). In the rotating cases, the rotation axis is parallel to the walls of the channel. Large-eddy simulation in a stationary square duct at a Reynolds number based on the friction velocity (Re_τ) of 300 is also reported and validated. In all the simulations the flow is assumed to be fully developed, incompressible and driven by an imposed pressure gradient. The Reynolds number for channel flows (Re_τ=194) was kept constant in the range of the rotational numbers studied ($0 \leq Ro_\tau \leq 3.6$). Computations were carried out using a second-order finite volume code with a localized one-equation dynamic subgrid scale (SGS) model. Forced heat advection (Pr=0.7) in a stationary channel has been conducted and compared with DNS results to check the ability of the SGS model used to correctly describe passive scalar transport. It has been found that the assumption of a constant SGS Prandtl number produces averaged temperature and turbulent heat fluxes profiles in agreement with existing DNS.

1. INTRODUCTION

Rotation effects in wall-bounded flows appear in many natural and engineering situations. Prediction of flow in rotating devices and, particularly, demanding blade cooling technology for industrial and aircraft turbines have motivated many of the existing studies dealing with rotating channel or duct flows. Fluid flow in most of these circumstances is turbulent, and the coupling of the rotation-induced forces on turbulence structure has been extensively studied in two-dimensional channels.

Physical phenomena occurring in turbulent channel flows subjected to spanwise rotation have been investigated experimentally (Johnston, 1972) and numerically (Miyake and Kajishima, 1986; Tafti and Vanka, 1991; Kristoffersen and Andersson, 1993; Piomelli and Liu, 1995; Lamballais et al., 1996 and Alvelius, 1999). Two main features arise when the axis of rotation is perpendicular to the plane of mean shear. First, it is well established that the interaction of the Coriolis force with the mean shear produces stabilization or destabilization of the flow near the two walls. Here, the concept of stability is related to an increase (destabilization) or with a decrease (stabilization) of the turbulence levels with respect to the non-rotating case. On the unstable side (or pressure side) of the channel, the mean shear vorticity is parallel to the rotation vector while, on the stable side (or suction side), these two vectors are anti-parallel. This situation can lead to the complete suppression of turbulence and the relaminarization of the flow on the stable side of the channel if the rotation rate is sufficiently high. A second effect of rotation is the development of longitudinal large-scale counter-rotating roll cells. These Taylor-Görtler vortices, analogous to those that develop due to the centrifugal instability arising from the streamline curvature, are localized on the unstable side but tend to drift along the spanwise and cross-stream directions and convect high momentum fluid towards the stable side.

Turbulent flow in a non-rotating duct with a rectangular cross-section is of engineering interest. It also has structurally remarkable features, especially near the corners where the flow has two inhomogeneous directions and where, on average, secondary flows of second kind occur. The mean structure of these flows in a cross-section of the duct consists of eight counter-rotating vortices which are distributed in pairs in the four quadrants and convect high momentum fluid from the central region of the duct to the corner region along the corner bisector. Low Reynolds number computations (Madabhushi and Vanka, 1991; Gavrilakis, 1992 and Huser and Biringen, 1993) show that secondary flows are relatively weak, with maxima of 2% of the mean axial velocity, but contribute considerably to the wall stress distributions. Huser and Biringen (1993) proposed an explanation of the mechanism for the generation of secondary flows based on quadrant analysis carried out with direct numerical simulations (DNS) data. According to these authors, the bursting events in the corners are suppressed by the reduced mean shear in the corner bisector. This, together with the fact that ejections of low momentum fluid from the walls generate a pair of streamwise counter-rotating vortices, results in the situation that the sense of rotation of the vortex closer to the corner determines the sense of rotation of the secondary circulation in that octant.

The Large-eddy simulation (LES) technique was chosen to keep the computational requirements at a moderate level. Previous numerical studies carried out to simulate turbulent flows in non-rotating ducts (Madabhushi and Vanka, 1991) and flows in rotating channel flows (Miyake and Kajishima, 1986; Tafti and Vanka, 1991 and Piomelli and Liu, 1995). showed the capability of the LES approach to give accurate results in these flows. The localized one-equation dynamic subgrid scale (SGS) model proposed by Kim and Menon (1997) was used in the present computations. The details on the SGS model are given in Section 2, where the physical and mathematical models are described. Validation of the simulations in

non-rotating channel and square duct flows and rotating channel flow are reported in Section 3.

2. MODEL

Figure 1 shows the physical model of the plane channel ($L_z = \infty$) and the straight square duct ($L_z = L_y$). The flow, driven by an externally imposed mean pressure gradient, is assumed to be fully developed and incompressible. The two walls of the infinite channel ($y = -L_y/2$ $y = L_y/2$) and the four walls of the duct ($y=0$, $y=L_y$, $z=0$, $z=L_z$) are rigid and smooth. The channel is rotating with respect to a fixed frame of reference with a constant positive angular velocity parallel to the z direction, $\vec{\Omega}=(0, 0, \Omega)$. Directions of the two components of the Coriolis acceleration are indicated in Figure 1.

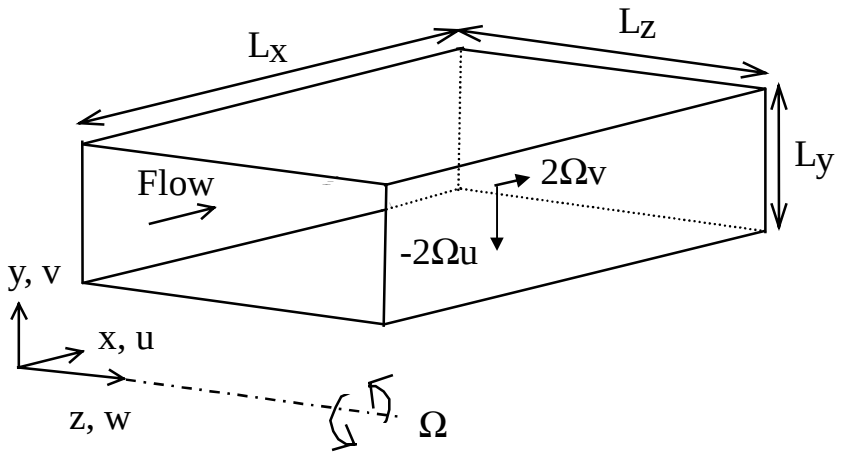

Figure 1. Physical model and coordinate system.

The flow is assumed to be hydrodynamically and thermally fully developed in the simulations of turbulent forced convection in a channel. The two walls of the channel are heated with a constant and uniformly distributed heat flux. The physical properties of the fluid with a Prandtl number of 0.7, are assumed to be constant with the temperature.

The large-eddy simulation technique is based on decomposition of the flow variables into a large-scale (or resolved) component and a subgrid scale

component. The resolved scales, denoted with a overbar, and the corresponding governing transport equations are defined by the filtering operation (Piomelli, 1993). The non-dimensional filtered continuity, Navier-Stokes and energy equations are

$$\frac{\partial \bar{u}_i}{\partial x_i} = 0, \tag{1}$$

$$\frac{\partial \bar{u}_i}{\partial t} + \frac{\partial \bar{u}_i \bar{u}_j}{\partial x_j} = -\frac{\partial \tau_{ij}}{\partial x_j} - \left(\delta_{1j} \frac{\partial P}{\partial x_i} + \frac{\partial \bar{p}}{\partial x_i} \right) + \frac{1}{Re_\tau} \frac{\partial^2 \bar{u}_i}{\partial x_j \partial x_j} + \in_{ij3} Ro_\tau \bar{u}_j \tag{2}$$

and

$$\frac{\partial \bar{\theta}}{\partial t} + \frac{\partial \bar{u}_i \bar{\theta}}{\partial x_j} = -\frac{\partial h_j}{\partial x_j} + \frac{4\bar{u}_1}{U_b} + \frac{1}{PrRe_\tau} \frac{\partial^2 \bar{\theta}}{\partial x_j \partial x_j} \tag{3}$$

respectively. The scales used to obtain the non-dimensional variables are the channel half-width ($D=L_y/2$) and the hydraulic diameter ($D=L_y=L_z$) as length scales for channel and square duct flow, respectively, and the average friction velocity (u_τ). For the forced convection channel flow simulations, the nondimensional temperature is defined as $\theta = (\langle Tw \rangle - T) \rho Cp\, u_\tau / q''_w$, where $\langle T_w \rangle$ is the wall temperature averaged along the spanwise direction as well as in time.

$$\langle T_w \rangle = \lim_{\Delta t \to \infty} \frac{1}{\Delta t} \int_{t=0}^{t=\Delta t} \left(\frac{1}{L_z} \int_{z=0}^{z=L_z} T_w \, dz \right) dt \tag{4}$$

Pressure has been scaled with the average wall stress, ρu_τ^2. In Equation (1), $\in_{ij3}$is the Levi-Civita's alternating tensor, $Re_\tau = u_\tau D/\nu$, $Ro_\tau = 2\Omega D/u_\tau$ and $Pr = \nu/\alpha$ are the Reynolds, the rotational and the Prandtl numbers, respectively. The first terms on the right hand side of Equations (2) and (3) are the contributions of the SGS stresses (τ_{ij}) and heat fluxes (h_j) to the resolved momentum and thermal energy transport, respectively.

According to the assumption of fully developed flow, the pressure and temperature fields (p* and T*) are decomposed into an averaged value which only depends on the streamwise coordinate (P and $\langle T_w \rangle$) and a fluctuating resolved term ($\bar{p}$ and $\bar{T}$), as shown in Equations (5) and (6).

$$p^*(x,y,z,t) = P(x) + \bar{p}(x,y,z,t) \tag{5}$$

$$T^*(x,y,z,t) = \langle T_w \rangle(x) + \bar{T}(x,y,z,t) \tag{6}$$

This decomposition allows the application of periodic boundary conditions for $\bar{u}_i$, $\bar{p}$ and $\bar{\theta}$ at $x = 0$ and $x = L_x$ and, thus, increase the sampling size to obtain averaged mean flow quantities and turbulence statistics.

The imposed mean pressure gradient along the streamwise direction is denoted in Equation (1) as $\delta_{1j} dP/dx_i$ ($dP/dx=-1$ for channel flow and $dP/dx=-4$ for duct flow). The second term on the right hand side of Equation 3, which arise from the above-mentioned decomposition of the temperature field, corresponds to the dimensional term, $u\, d\langle T \rangle_w / dx$. The macroscopic thermal energy balance, for a fully developed flow and thermal field, indicates that the wall temperature ensemble-averaged over the z-direction increases linearly along the x-direction.

$$d\langle T \rangle_w / dx = dT_b / dx = 4q''_w / \rho Cp U_b \tag{7}$$

In Equation (7), U_b and T_b are the bulk velocity and the bulk temperature, respectively, which are defined as

$$U_b = \frac{1}{S} \int_S u \, dS \tag{8}$$

$$T_b = \frac{1}{U_b S} \int_S u T \, dS \tag{9}$$

where S is the cross sectional area of the channel (S=Ly Lz).

The subgrid scale stresses (τ_{ij}) have been computed following the localized one-equation dynamic SGS model developed by Kim and Menon (1997). A brief description of the model is given in the following. The SGS stress tensor is modeled as

$$\tau_{ij} = -2 C_\tau \bar{\Delta} k_{sgs}^{1/2} \bar{S}_{ij} + \frac{1}{3} \delta_{ij} \tau_{kk} \tag{10}$$

where C_τ is a coefficient to be computed dynamically, $\bar{\Delta}$ is the characteristic subgrid scale energy length (or grid scale), k_{sgs} is the subgrid scale kinetic energy and $\bar{S}_{ij}$ is the resolved strain tensor. The second term on the left-hand side of Equation (10) is included in the pressure term. The subgrid scale kinetic energy (k_{sgs}) is obtained by solving its transport equation (see Kim and Menon, 1997), in which the dissipation term (ε_{sgs}) is modeled as

$$\varepsilon_{sgs} = \frac{C_\varepsilon k_{sgs}^{3/2}}{\bar{\Delta}} \tag{11}$$

where C_ε is another coefficient also determined dynamically.

The procedure for computing the localized values of the model coefficients, C_τ and C_ε, is based, as in other localized dynamic SGS models (Piomelli, 1993) on the definition of a test scale field. The test filter, characterized by $\hat{\Delta}$ and equal to $2\bar{\Delta}$, and applied to any variable $\bar{\phi}$, is denoted by $\hat{\bar{\phi}}$. The experimentally measured similarity (Liu et al. 1994) between the test scale Leonard stresses, $L_{ij} = \left(\widehat{\bar{u}_i \bar{u}_j} - \hat{\bar{u}}_i \hat{\bar{u}}_j\right)$, and the SGS stresses allows a reasonable assumption of the same parameterization for both tensors, τ_{ij} and L_{ij}

$$L_{ij} = -2\, C_\tau \hat{\Delta} k_{test}^{1/2} \hat{\bar{S}}_{ij} + \frac{1}{3}\delta_{ij} L_{kk} \tag{12}$$

where L_{ij} is the resolved kinetic energy at the test scale. The over-determined model coefficient C_τ in Equation (12) can be computed from resolved quantities at the test filter level, using the least-square minimization procedure.

$$C_\tau = \frac{1}{2}\frac{L_{ij}\hat{\bar{S}}_{ij}}{\hat{\bar{S}}_{ij}\hat{\bar{S}}_{ij}} \tag{13}$$

The dissipation rate of the test scale kinetic energy at the small scales is produced by the molecular (ν) and the SGS viscosity (ν_{SGS}) and can be written as

$$\varepsilon_{test} = (\nu + \nu_{SGS})\left[\left(\widehat{\frac{\partial \bar{u}_i}{\partial x_j}\frac{\partial \bar{u}_i}{\partial x_j}}\right) - \left(\frac{\partial \hat{\bar{u}}_i}{\partial x_j}\frac{\partial \hat{\bar{u}}_i}{\partial x_j}\right)\right] \quad (14)$$

Similarity between the dissipation rates at the grid filter level (ε_{sgs}) and the test filter level (ε_{test}) is also invoked, and the dissipation model coefficient (C_ε) is computed as

$$C_\varepsilon = \frac{\hat{\Delta}\varepsilon_{test}}{k_{test}^{3/2}} \quad (15)$$

This model, based on the similarity between the SGS stress tensor and the test scale Leonard stress tensor, overcomes the numerical stability problems of the earlier dynamic models without any averaging or adjustment of the model coefficients because the denominators of Equations. (13) and (15) have well defined quantities. This is an important feature when simulating turbulent flows under rotation because of the stabilizing/destabilizing effects of rotation on turbulence. Kim and Menon (1997) examined the properties of the model by conducting LES of turbulent flows such as decaying, forced and rotating isotropic turbulence, turbulent mixing layer and plane Couette flow. Their results showed good agreement with existing experimental and DNS data.

As shown in Cabot and Moin (1993), who computed $Pr_{SGS}=\nu_{SGS}/\alpha_{SGS}$ from DNS data of forced convection channel flow at Pr=0.7, Pr_{SGS} tends to reach relatively constant values at large times and in the central region of the channel ($Pr_{SGS}\approx 0.4$). Consequently, the SGS heat fluxes, h_j, in Equation (3) have been computed by assuming constant SGS Prandtl number (Pr_{SGS} =0.4)

$$h_j = -\frac{\nu_{SGS}}{Pr_{SGS}}\frac{\partial \bar{\theta}}{\partial x_j} \quad (16)$$

The governing transport equations [Equations. (1 to 3)] were solved numerically with the CALC-LES code (Davidson, 1997). This second-order accuracy finite volume code uses central differencing of the diffusive and convective terms on a collocated grid and a Crank-Nicolson scheme for

the temporal discretization. The coupling between the velocity and pressure fields is solved efficiently by means of an implicit, two-step, time advancement method and a multigrid solver for the resulting Poisson equation (Emvin, 1997). This code has several optional SGS models implemented and has been successfully tested in simulating various transitional and turbulent flows of engineering interest such as flow around obstacles (Krajnovic and Davidson, 1999; Sohankar et al. 1999 and Sohankar, 2000) and buoyancy-driven and forced convection recirculating flows in enclosures (Peng, 1997).

The computational domain was divided into 66x66x66 grid nodes for the channel and duct flow simulations. They were uniformly distributed along the homogeneous directions ($\Delta x^+ \approx 37$ and $\Delta z^+ \approx 9$ for the channel and $\Delta x^+ \approx 29$ for the square duct) in which periodic boundary conditions were imposed, while tanh distributions were used to stretch the nodes near the walls where the no-slip condition was applied. For the Reynolds numbers considered, the minimum and maximum grid spacing in the directions perpendicular to the walls are $(\Delta y^+)_{min} \approx 0.7$ and $(\Delta y^+)_{max} \approx 11$ for the channel flow ($Re_\tau = 194$) and $(\Delta y^+)_{min} = (\Delta z^+)_{min} \approx 0.4$ and $(\Delta y^+)_{max} = (\Delta z^+)_{max} \approx 9$ for the square duct flow ($Re_\tau = 300$). A constant wall temperature, $\theta_w = 0$, was imposed at the four walls when simulating forced convection channel flow.

3. RESULTS

Simulations of the isothermal stationary channel and duct flows started from laminar velocity distributions at the final Reynolds numbers (Re_τ=194 for channel flow and Re_τ=300 for duct flow). With time, the flow progressively and spontaneously became turbulent. The sampling procedure used to obtain the average velocity fields and the turbulent intensities was not started until the flow was statistically fully developed. Results at the lowest rotation rate (Ro_τ=1.5) were obtained starting from an instantaneous isothermal non-rotating flow field until a new statistically steady state was reached. The rotation number was increased from 0 to 1.5 and from 1.5 to 3.6 maintaining a constant imposed pressure gradient (i.e. constant value of Re_τ). The computed mean wall stress (τ_w) is balanced by the imposed pressure gradient within 0.05% in all the simulations reported in this work. Instantaneous fully developed velocity and pressure fields of channel flow were used as initial condition for the forced convection simulation. The initial temperature field was computed from the instantaneous streamwise velocity component using the analogy between the momentum and heat transfer in the viscous sublayer (θ=Pr u). The bulk velocity in Equation (3) was computed from the isothermal channel flow simulations (U_b=15.9).

The sampling procedure used to obtain the average velocity fields and the turbulent intensities and heat fluxes was not started until the flow and thermal fields were statistically fully developed. The flow quantities were averaged along the homogeneous directions as well as in time, typically over about 15 and 40-70 non-dimensional time units for channel and duct flows, respectively.

Table I summarizes the characteristics of rotating and non-rotating channel and square duct flow studies used to validate the present simulations. In the following discussion, the averaged resolved velocities, turbulent stresses

and turbulent heat fluxes are denoted as U_i, $\langle u_i' u_j' \rangle$ and $\langle u_i' \theta' \rangle$, respectively, for simplicity.

	Authors	Grid points x y z	Domain Lx Ly Lz	Re_τ (u_τ D/ν)	Ro_τ ($2\Omega D/u_\tau$)
Isothermal channel flow	Kim et al. (1987)*[1]	192x129x160	4πx2x2π	180	0
	Piomelli (1993)	48x65x64	4πx2xπ	200	0
	Kristoffersen & Andersson (1993)*	128x128x128	4πx2x2π	194	$-7.5 \le Ro_\tau \le 0$
	Alvelius (1999)*	384x129x240	8πx2x3π	180	$0.1 \le Ro_\tau \le 7.3$
	Present	66x66x66	4πx2xπ	194	0, 1.5, 3.6
Forced convection channel flow (Pr=0.71)	Kasagi et al. (1992)[1]	128x97x128	5πx2x2π	150	0
	Kawamura et al. (1999)[2]	128x66x128	3πx2x2π	180	0
	Present	66x66x66	4πx2xπ	194	0
Duct flow	Gavrilakis (1992)*	1000x127x127	10πx1x1	300	0
	Present	66x66x66	2πx1x1	300	0

Table I. Characteristics of direct* and large-eddy simulations.

[1]Data available at: `http://cfd.me.umist.ac.uk/ercofold/database/homepage.html`

[2]Data available at: `http://muraibm.me.noda.sut.ac.jp/homepage/e-database1.html`

Figures 2a and 2b show the streamwise mean velocity (U) profile along the vertical direction and the computed turbulence intensities in the non-rotating channel flow, respectively. It can be seen that the present results are in good agreement with the DNS of Kim et al. (1987) and LES of Piomelli (1993). The predicted non-dimensional centerline velocity is 18.2, the same value reported by Kim et al. (1987) and the dimensionless bulk velocity (U_b=15.9, $Re=2Re_\tau U_b$=6170) is 1.7% higher than the DNS results. The computed friction factor ($f= 2\tau_w/\rho$ =0.0078) is within 5% of the correlation of experimental data (Dean, 1978).

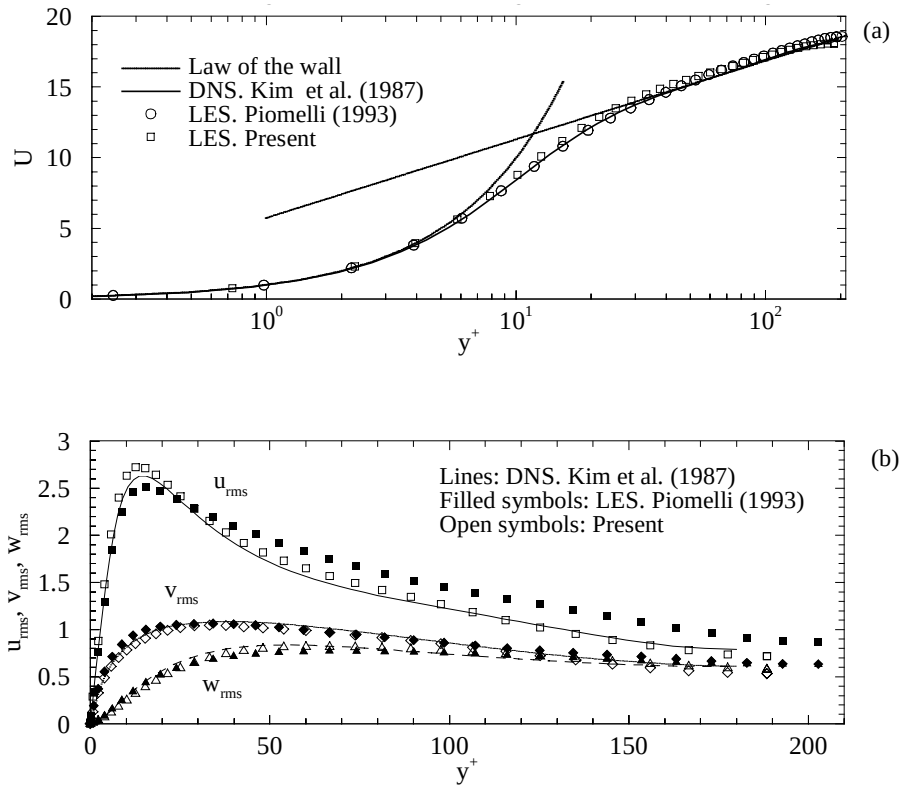

Figure 2. Averaged velocity (a) and turbulence intensities (b) profiles in non-rotating channel flow.

The results of Piomelli (1993) were obtained using the dynamic SGS model of Germano et al. (1991) to compute the model coefficient. This procedure assumes the model coefficient to be a function only of time and inhomogeneous directions, C(y,t). It can be seen that the u_{rms} values in the logarithmic layer are better reproduced by the present predictions. This may be attributed to the slightly higher grid resolution in the streamwise direction of the present simulations (see Table I). However, the fact that the LES of Piomelli (1993) were conducted with a higher accuracy code seems to indicate that the difference may be connected with a better performance of the Kim and Menon (1997) SGS model.

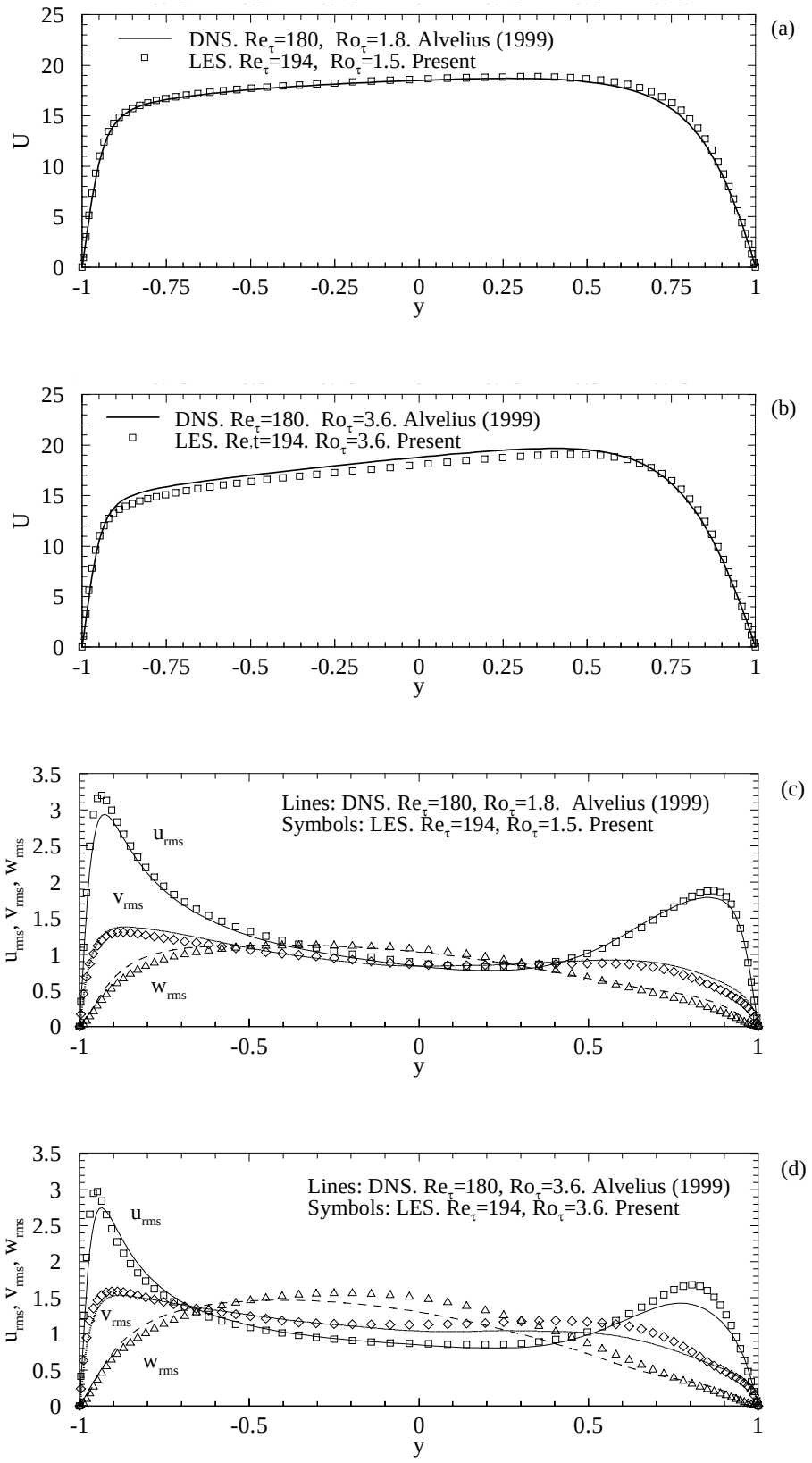

Figure 3. Averaged velocity (a and b) and turbulence intensities (c and d) in rotating channel flow.

Figures 3a and 3b show the mean streamwise velocity and turbulence intensities' vertical profiles of rotating channel flow at Ro_τ=1.5, respectively. The DNS of Alvelius (1999) at Ro_τ=1.8 and Ro_τ=3.6 were selected for the comparison because the computational domain used by this author is the largest of the rotating channel flow studies shown in Table I and has the same grid resolution as the DNS of Kim et al. (1987). Good agreement is found when comparing, in Figure. 3, the DNS of Alvelius (1999) and the present results. As shown in Figures 3a and 3b, the average velocity profile becomes asymmetric as the rotation number is increased. It can be seen in Figures 3a and 3b that the present predictions accurately reproduce the quasi-linear region of the profile U(y), where the absolute mean vorticity, $-(dU/dy)+Ro_\tau$ becomes approximately zero (see Kristoffersen and Andersson, 1993)

Figures 3b and 3d show that Reynolds stresses are generally reduced in comparison with the non-rotating case (Figure 2b) on the stable side (near the stable wall, y=1) and that they are generally increased on the unstable side (near the unstable wall, y=-1). Detailed analyses of the effects of rotation on the different Reynolds stresses based on the generation terms of the transport equations, are reported in Johnston et al. (1972) and Kristoffersen and Andersson (1993).

Comparison of averaged temperatures and heat fluxes in forced convection flow at Re_τ=194 (Re=6170) and Pr=0.7 are shown in Figure 4. It can be seen that a good agreement is found comparing the present LES obtained with a constant Pr_{SGS} number and DNS data of Kasagi et al. (1992) and Kawamura et al. (1998). The value of the Nusselt number (Nu=20.7) is a 5% larger than the one predicted by the Gnielisky's correlation (Gnieliski, 1976).

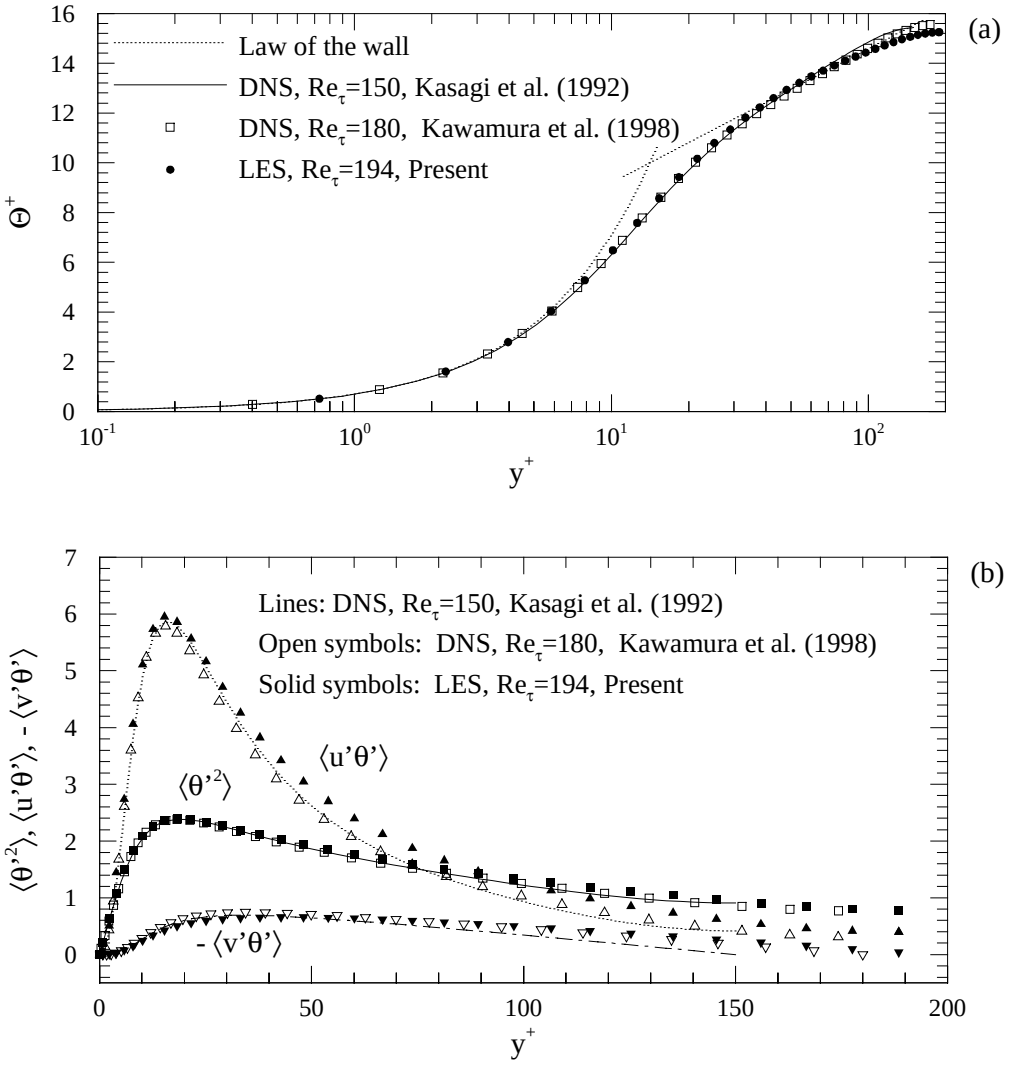

Figure 4. Averaged temperature (a) and turbulent heat fluxes (b) profiles in non-rotating channel flow

Turbulent flow in a non-rotating square duct was simulated at Re_τ=300 and the results compared with DNS of Gavrilakis (1992) at the same value of Re_τ and experiments of Cheesewright et al. (1990) at Re_c=4900, based on the centerline velocity, which is close to the value in the present computation (Re_c=5900).

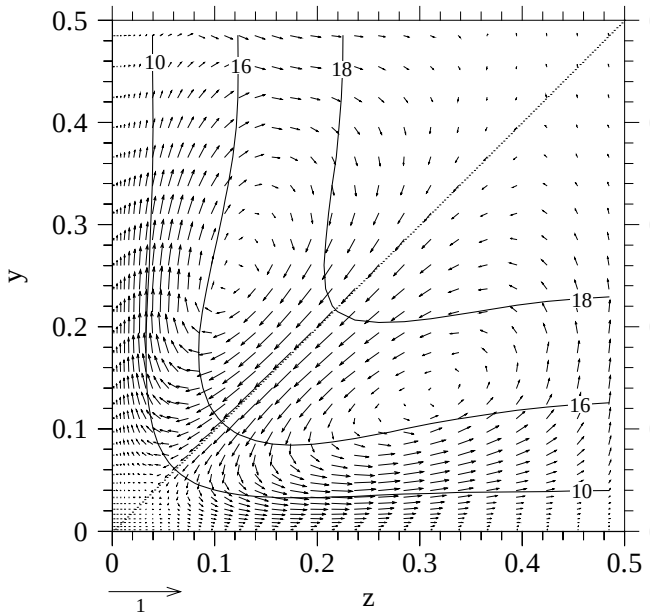

Figure 5. Averaged flow field in a non-rotating square duct in terms of contours of the streamwise velocity component and cross-stream vector field. The vector near the bottom right corner has a length of 1.

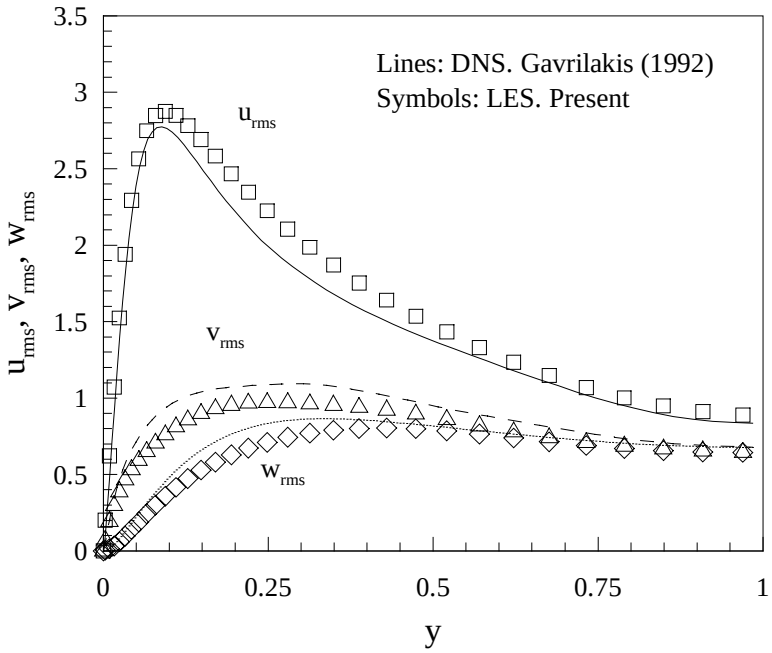

Figure 6. Averaged turbulent intensity profiles along the wall bisector (z=0.5) in non-rotating duct flow at Re_τ=300.

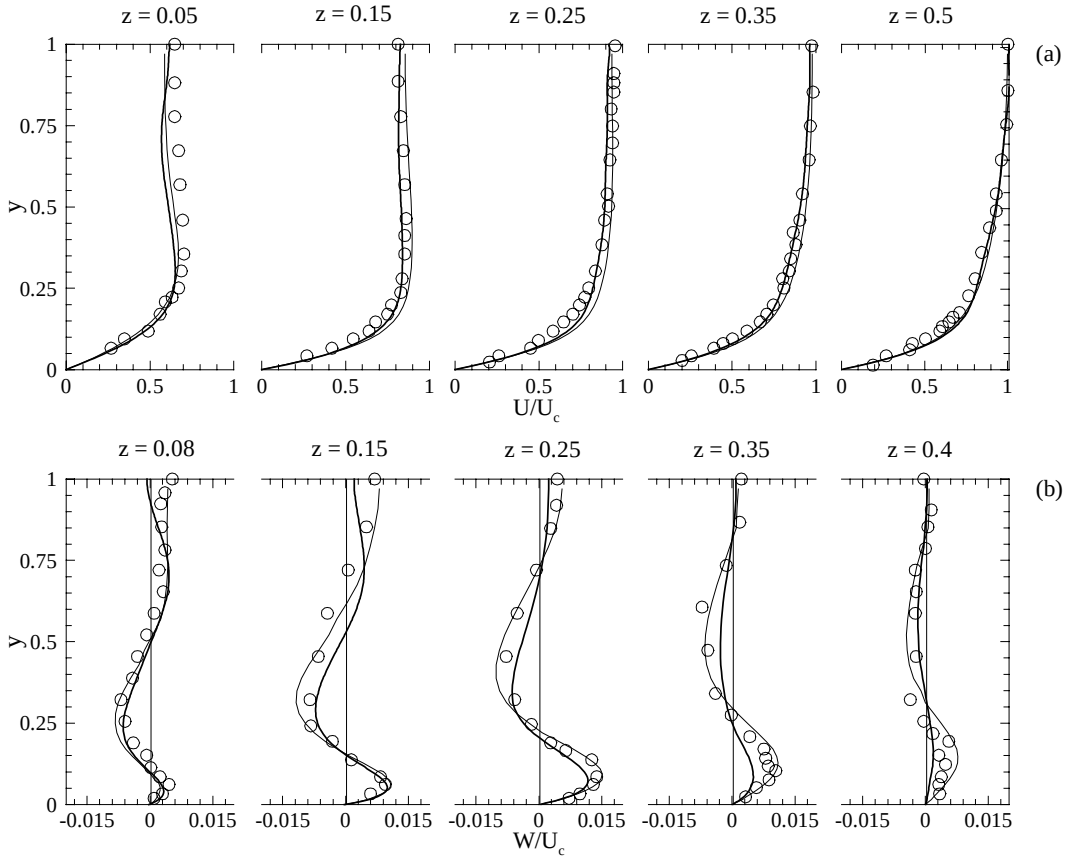

Figure 7. Averaged streamwise (a) and spanwise (b) velocity profiles in a square duct. Symbols: LDV measurements of Cheesewright et al. (1990). Thick lines: DNS of Gavrilakis (1992). Thin lines: LES present.

Figure 5 shows the contours of the mean axial velocity component (U) together with the averaged vector field defined by the cross-stream components (V and W). Time and streamwise averaged velocity fields were also averaged in the eight octants of the cross-section. The time and streamwise averaged field of the axial velocity component is symmetric with respect to the octant average within 3%. It can be seen in Figure 5 that the distortion of the U contours towards the corner indicates momentum transfer by the secondary flows from the central part of the duct towards the corners. Gavrilakis (1992) reported a small flow cell near the wall bisector with a dimension of about L/D=0.08. Figure 5 does not reveal the presence of this cell, probably because of the relatively large grid spacing in this region ($\Delta z \approx 0.03$). The Reynolds number based on the bulk velocity and the hydraulic diameter is 4500, which is 2% higher than the value

calculated by Gavrilakis (1992). The predicted friction factor (f=0.0093) is the same as that obtained with Dean's correlation for ducts (Dean, 1978). The volume averaged turbulent kinetic energy, 2.14, agrees well with that reported by Gavrilakis (1992), 2.1. Figure 6 shows the profiles of the normal turbulent stresses along the wall bisector (z=0.5). The maximum value of the averaged secondary velocities (≈0.3) is well below the magnitude of the rms values shown in Figure 6. Figures 7a and 7b show the vertical profiles of the axial and cross-stream velocities at different horizontal positions. The centerline velocity (U_c) was adopted as the velocity scale in these figures because it is the only one available in the experiments of Cheesewright et al. (1990). Good agreement is found when comparing present predictions of the velocity fields (Figures 7a and 7b) and the turbulence statistics (Figure 6) along the wall bisector with DNS and experiments.

4. CONCLUSIONS

Fully developed turbulent flows at low Reynolds numbers in stationary and rotating channels as well as in a non-rotating square duct have been simulated using a second order code with a one-equation dynamic subgrid scale model. Present predictions of the averaged velocity and turbulent stresses are in good agreement with existing direct numerical simulations. Large-eddy simulations of turbulent forced convection flows in a stationary channel have been also conducted. It has been found that the assumption of constant subgrid scale Prandlt number reproduces accurately the averaged temperature and turbulent heat fluxes of available direct numerical simulations.

AKNOWLEDGMENTS

This work was conducted during the first author stay at the Department of Thermo and Fluid Dynamics (Chalmers University of Technology). The support of SEUID (Ministry of Education and Technology of Spain) is gratefully aknowledged. We would like to thank S. Gavrilakis, K. Alvelius and A. Johansson for providing us the data from their simulations.

REFERENCES

Alvelius K. (1999) Studies of turbulence and its modeling through large eddy- and direct numerical simulation PhD thesis, Dept. of Mechanics, Royal Institute of Technology, Stockholm

Cabot W. and Moin P. "Large eddy simulations of scalar transport with the dynamic subgrid-scale model" in *Large eddy simulation of complex engineering and geophysical flows.* B. Galperin and S. A. Orszag, editors. Cambridge University Press, 1993

Cheesewright R., McGrath G. and Petty D. G. (1990) LDA measurements of turbulent flow in a duct of square cross section at low Reynolds number *Aeronautical Engineering Dept. Rep. ER 1011*. Queen Mary Westfield College. University of London.

Davidson L. (1997) LES of recirculating flow without any homogeneous direction: A dynamic one-equation subgrid model, in *2nd Int. Symp. on Turbulence Heat and Mass Transfer*, Delft, Delft University Press. pp 481-490

Dean R. B. (1978) Reynolds number dependence of skin friction and other bulk flow variables in two-dimensional rectangular duct flow *J. Fluids Eng*. **100**, 215

Emvin P. (1997) The full multigrid method applied to turbulent flow in ventilated enclosures using structured and unstructured grids, PhD thesis, Dept. of Thermo and Fluid Dynamics, Chalmers University of Technology, Gothenburg

Gavrilakis S. (1992) Numerical simulations of low-Reynolds-number turbulent flow through a straight square duct *J. Fluid Mech.* **244**, 101

Germano M., Piomelli U., Moin P. and Cabot W. H. (1991) A dynamic subgrid-scale eddy viscosity model," *Phys. Fluids A* **3**, 1760

Gnielisky V. (1976) New equations for heat and mass transfer in turbulent pipe and channel flow, *Int. Chem. Eng*. **16**, 359.

Huser A. and Biringen S. (1993) Direct numerical simulation of turbulent flow in a square duct *J. Fluid Mech*. **257**, 65

Johnston J. P., Hallen R. M. and Lezius D. K. (1972) Effects of spanwise rotation on the structure of two-dimensional fully developed turbulent channel flow *J. Fluid Mech.* **56**, 533

Kasagi N., Tomita Y. and Kuroda A. (1992) Direct numerical simulation of passive scalar field in a turbulent channel flow *J. Heat Transfer* **114**, 598

Kawamura H., Abe H. and Matsuo Y. (1999) DNS of turbulent heat transfer in channel flow with respect to Reynolds and Prandtl number effect *Int. J. Heat and Fluid Flow* **20**, 196.

Kim J., Moin P. and Moser R. (1987) Turbulence statistics in fully developed channel flow at low Reynolds number *J. Fluid Mech*. **177**, 133

Kim W. and Menon S. (1997) Application of the localized dynamic subgrid-scale model to turbulent wall-bounded flows, AIAA Paper 97-0210. *35th Aerospace Sciences Meeting & Exhibit*, Reno, NV

Krajnovic S. and Davidson L. (1999) Large-eddy simulation of the flow around a surface-mounted cube using a dynamic one-equation subgrid model, *1st Int. Symp. on Turbulence and Shear Flow Phenomena*, Santa Barbara.

Kristoffersen R. and Andersson H. (1993) Direct simulations of low-Reynolds-number turbulent flow in a rotating channel *J. Fluid Mech.* **256**, 163

Lamballais E., Lesieur M. and Métais O. (1996) Effects of spanwise rotation on the vorticity stretching in transitional and turbulent channel flow *Int. J. Heat and Fluid Flow*, **17**, 324

Liu S., Meneveau C. and Katz J. (1994) On the properties of similarity subgrid-scale models as deduced from measurements in a turbulent jet *J. Fluid Mech.* **275**, 83

Madabhushi R. V. and Vanka S. P. (1991) Large-eddy simulation of turbulence-driven secondary flows in a square duct *Phys. Fluids A* **3**, 2734

Miyake Y. and Kajishima T. (1986) Numerical simulation of the effect of Coriolis force on the structure of turbulence *Bulletin of JSME*. **29**, 3341

Peng S. (1997) Modelling of turbulent flow and heat transfer for building ventilation, PhD thesis, Dept. of Thermo and Fluid Dynamics, Chalmers University of Technology, Gothenburg.

Piomelli U. (1993) High Reynolds number calculations using the dynamic subgrid-scale stress model *Phys. Fluids A* **5**, 1484

Piomelli U. and Liu J. (1995) Large-eddy simulation of rotating channel flows using a localized dynamic model," *Phys. Fluids A* **7**, 839

Sohankar A., Davidson L. and Norberg C. (2000) Large eddy simulation of flow past a square cylinder: Comparison of different subgrid scale models, *J. Fluids Eng*. **122**, 39. See also Erratum, *J. Fluids Eng*. **122**, 643

Sohankar A., Norberg C. and Davidson L. (1999) Simulation of three-dimensional flow around a square cylinder at moderate Reynolds numbers *Phys. Fluids A* **11**, 288

Tafti D. K. and Vanka S. P. (1991) A numerical study of the effects of spanwise rotation on turbulent channel flow *Phys. Fluids A* **3**, 642